Asymmetric flows over symmetric surfaces: capacitive coupling in induced charge electro-osmosis

by

Tobias S. Mansuripur

A Dissertation submitted in partial satisfaction of the

requirements for the degree of

Bachelor of Science

in

Physics

in the

COLLEGE OF CREATIVE STUDIES

of the

UNIVERSITY OF CALIFORNIA, SANTA BARBARA

Thesis Advisor:

Professor Todd Squires

Spring 2009

The dissertation of Tobias S. Mansuripur is approved:

Professor Todd Squires Date

Dr. Ilan Ben-Yaacov Date

Abstract

We report curious asymmetric induced-charge electro-osmotic (ICEO) flows over a symmetric, planar gate electrode under applied AC electric fields, whereas symmetric, counter-rotating rolls are expected. Furthermore, the asymmetric component of the flow is consistently directed towards the grounded electrode. We propose that capacitive coupling of the gate electrode to the microscope stage–a comparatively large equipotential surface that acts effectively as a ground–is responsible for this symmetry breaking. This stray capacitance drives the formation of a double layer whose zeta potential is proportional to the potential drop from the electrolyte directly above the gate electrode to the external stage. Therefore, the charge in this "stray" double layer varies in phase with the driving field, resulting in a rectified, steady flow as with standard ICEO. We experimentally vary the stray capacitance, the electric potential of the stage, and the location of the gate electrode, and find that the effect on the stray flow is consistent with the predictions of the proposed mechanism. In the process, we demonstrate that capacitive coupling offers an additional means of manipulating fluid flow over a polarizable surface.

Acknowledgements

This work was supported by the National Science Foundation, under CBET CAREER grant 0645097, and REU supplements 0741381 and 0836263. Microfabrication was performed in the UCSB nanofabrication facility, part of the NSF-funded NNIN network. I gratefully acknowledge Steve Wereley, for providing his micro-PIV codes. I especially thank Andy Pascall for teaching me microfabrication and for his patience in answering my many questions, without whom this project never would have gotten anywhere. Most of all, I thank Todd Squires for the opportunity to do research in his lab, and for allowing me the freedom to pursue interesting tangents.

Contents

1 Introduction

Recent years have seen intense interest in microfluidic systems [1, 2, 3], which, in turn, has spurred a resurgence in electrokinetics for micron-scale flow manipulation. In particular, electro-osmotic flows occur when the thin (typically $\sim 1-10$ nm) ionic clouds that screen charged surfaces are forced into motion by an applied electric field E. The surrounding fluid is dragged along with the ions, establishing an electro-osmotic "slip" velocity given by Smoluchowski's classic formula

$$u = -\frac{\epsilon\zeta}{\eta}E, \tag{1}$$

where ϵ and η are the permittivity and viscosity of the electrolyte solution, and ζ is the electrostatic potential drop across the diffuse part of the ionic screening cloud [4, 5].

Recent interest has been especially keen in the development of nonlinear electrokinetic phenomena, such as AC electrokinetics (ACEK) [6, 7], induced charge electrokinetics (ICEK) [8, 9], nonlinear electrokinetic instabilities [10, 11, 12], and ACEK micropumps [13, 14, 15]. The nonlinearity of these phenomena arises when the (applied) electric field *induces* an ionic charge cloud around a polarizable surface, then subsequently drives the induced charge into motion. Under AC applied fields at sufficiently low frequencies ω, the electric field and induced zeta potential ζ_i vary *in phase*, giving a non-zero, rectified steady flow. By contrast, the standard equilibrium double layer is presumed to be static in time, so that the standard electro-osmotic

flow that results from an oscillatory applied field simply time-averages to zero. In particular, if one assumes that the induced double layer ($\zeta_i \sin \omega t$) and equilibrium double layer (ζ_{eq}) simply superpose, which is reasonable at least in the limit $|\zeta_i + \zeta_{eq}| \ll k_B T/e$, then

$$\langle u_s \rangle = -\frac{\epsilon}{\eta} < (\zeta_i \sin(\omega t) + \zeta_{eq}) E \sin(wt) >= -\frac{\epsilon \zeta_i E}{2\eta}, \tag{2}$$

In other words, only the induced double layer contributes to steady flow.

Most ICEK studies [9, 8, 16, 17], as well as earlier work involving metal colloids (*e.g.* [18, 19]) have involved cylinders and spheres. Instead, we use a planar system (Fig. 1) that allows the ICEO slip velocity to be measured directly [20]. A thin, metal "gate" electrode is deposited on the glass surface at the bottom of a microfluidic channel. The electric field in the channel is applied through two driving electrodes: the "powered" electrode carries the applied voltage and the "grounded" electrode is held at electrical ground.

Figure 2 illustrates the basic physics behind ICEO. An electric field that is applied *along* the channel polarizes the gate electrode. Ions in solution are driven along the electric field lines, with positive ions driven towards one half of the gate electrode, and negative ions driven toward the other half. Under "ideally polarizable" conditions, no current passes through the electrolyte/metal surface, and instead the ions that arrive form an induced double layer, whose zeta potential varies with position along the gate electrode. Since the gate electrode–a floating conductor–is electrically isolated,

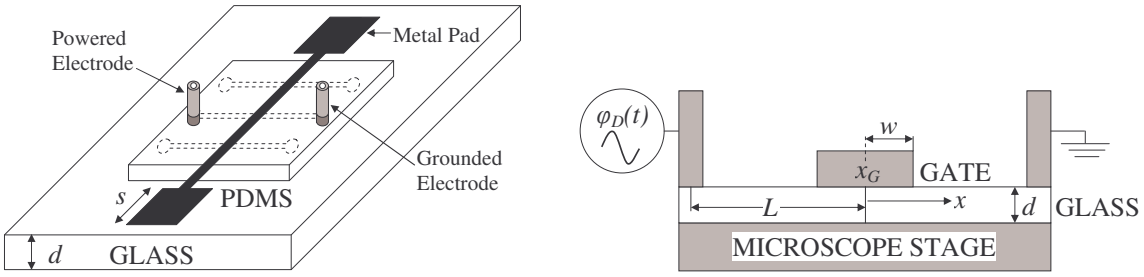

(a) (b)

Figure 1: (a) The experimental device. The PDMS containing the channels is bonded to the glass slide, with the driving electrodes in each end of the channel. The gate electrode is connected to the metal pads, whose area is given by $A_P = 2s^2$. (b) Channel cross-section. The coordinate x originates at the center of the channel, and the gate electrode is centered at x_G. The length of the channel is $2L$ and the width of the gate electrode is $2w$. The gate electrode and pads are separated from the microscope stage by the glass slide of thickness d. The powered electrode is taken to be on the left, and the grounded electrode on the right.

its total charge is fixed. The *induced* zeta potential, which is the only component that drives a non-zero flow in an AC field, must therefore contain zero net charge. Consequently, the *spatially* averaged flow over the gate electrode,

$$\int \langle u_s \rangle dA = -\frac{\epsilon}{\eta} E \int \zeta_i dA = 0, \tag{3}$$

should vanish. Given that the electrode and the solution are symmetric, and that an AC field is applied, one should expect quite generally that the time-averaged ICEO flow should be *symmetric*, with slip velocities directed towards the center of the electrode, driving two rolls of fluid in the bulk

above.

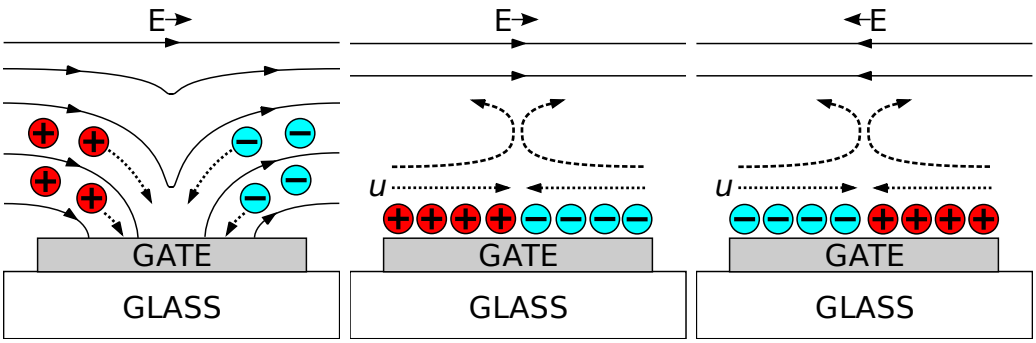

(a) (b) (c)

Figure 2: (a) When the electric field is first applied, the field lines intersect the gate electrode perpendicularly and begin to drive ions from the solution onto the gate. (b) Once the double layer is fully formed, the electric field is screened from the gate electrode and directed parallel to the electrode surface, along the channel in the bulk of the solution. The ions in the double layer are driven by the field and achieve a slip velocity u, shown by the dotted line. The dashed line shows the resulting counter-rotating rolls in the bulk of the channel. (c) On the second half of the AC cycle, the electric field points in the opposite direction and the ions in the double layer switch sides. Therefore, the force on the double layer is rectified, which results in a steady, non-zero time average flow.

Herein, we investigate a curious observation in the planar ICEO system. During experiments, we frequently observe a time-averaged *asymmetric* flow over the gate electrode, giving a net flow over the gate electrode in a particular direction. This stands at odds with the symmetric flow one would naturally expect from this symmetric system. Moreover, the net drift velocity always appears to be directed towards the grounded electrode: switching the leads (*i.e.* switching which electrode is powered, and which is grounded) *reverses*

the direction of the flow asymmetry. Similar asymmetries have been observed in other ICEO experiments [20], and in AC electrohydrodynamic experiments [21].

We propose that the mechanism responsible for these asymmetric flows involves a capacitive coupling between the gate electrode and the "external" experimental apparatus. For example, the experiments described here are performed atop a metal microscope stage and objective, which behave effectively as an electrical ground. In our original description, charge flows left-right only; in the full system, however, charge can flow *along* the electrode, from the portion of the gate that contacts the electrolyte (and which thus forms a double-layer) to the portion whose capacitive coupling with the outside world is strongest (Fig. 3(a)). In the above discussions, only the potential gradient along the channel has been considered, and therefore the ICEO slip velocity is assumed to be independent of the absolute potential above the gate electrode. Given that the apparatus is an effective ground, however, the potential must drop from its value in the bulk electrolyte ϕ_B to zero at the microscope stage. In response to this voltage drop, the solution forms a uniform "stray" double layer over the gate electrode. Because this stray double layer is induced by the field, it varies *in phase* at sufficiently low frequencies, and it also gives rise to a non-zero, time-averaged flow just like ICEO (Fig. 3(b)). When all double layers are accounted for, the result is a uniform flow superposed on a symmetric ICEO flow (Fig. 3(c), 3(d)), which breaks the expected symmetry. In particular, as detailed below, one expects

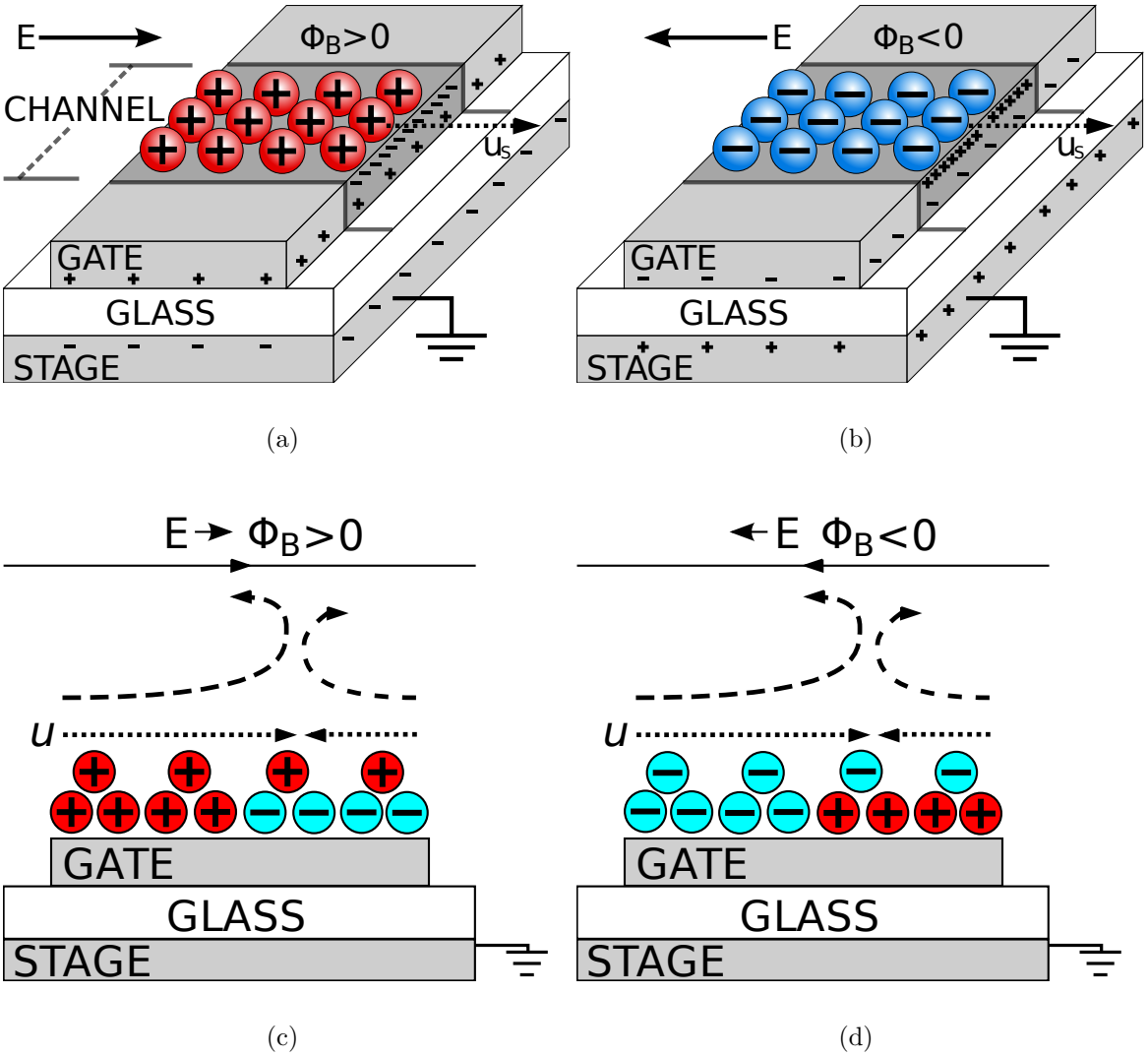

Figure 3: Formation of the stray double layer. With the powered electrode on the left and the grounded electrode on the right (not shown, see fig. 1), the potential of the bulk solution above the gate is positive when the electric field points to the right (a) and a positively charged double layer forms. When the electric field switches directions (b), the stray double layer is negatively charged, but the force is consistently directed towards the grounded electrode. The superposition of the standard ICEO double layer and stray double layer are shown in (c) and (d) for opposite phases of the electric field.

the stray flow to be directed towards the grounded electrode quite generally, as observed in experiments.

The effect we report here involves a modulation of the ζ-potential above the gate electrode via capacitive coupling with the external apparatus (here passively, later through actively controlling the potential of the stage). An analogous 'field-effect' flow control via external modulation of ζ has been demonstrated in the so-called flow-FET, both DC [22, 23, 24, 25] and AC [26]. Below we discuss similarities and differences between these two systems.

In what follows, we develop a simple, predictive theory for the effect of stray capacitance upon ICEO flows, and the asymmetric flows that one should expect. The velocity of the stray flow is shown to depend upon the magnitude of the stray capacitance, and the potential drop between the electrolyte directly above the gate and the microscope stage. We then test our theory by experimentally varying the following three quantities and measuring the resulting asymmetric flow: (i) We vary the electrostatic potential of the electrolyte (but not its gradient) above the gate by changing the relative position of the gate electrode between the powered and driving electrodes. (ii) We control the geometric size of the stray capacitor–and thus its capacitance–by adding metal pads to the gate electrode. (iii) We directly vary the potential of the microscope stage itself, demonstrating that the asymmetry can be enhanced, reversed or eliminated with an electrified stage. In particular, setting the potential of the microscope stage equal to the potential in the bulk solution over the gate electrode eliminates the asym-

metric flow completely, regardless of the magnitude of the stray capacitance. There is a sizeable quantitative disparity between the predicted and measured stray flow velocities; however, such discrepancies are ubiquitous in ICEO experiments [20]. By normalizing our measured ICEO velocities relative to a reference measurement, however, we scale out any constant discrepancy, and find the relative flows show strong quantitative agreement with the theory.

2 Theory

ICEK phenomena result when a charge cloud is induced on a polarizable surface by an applied electric field, and subsequently driven by that same field [8, 9]. In the discussion that follows, all ICEO equations and diagrams will be pertinent to the planar geometry, shown in Fig. 1, that was used in experiments. The channel, of length $2L$, is filled with an electrolyte solution. The coordinate x describes the position in the channel, where the origin is chosen to be the midpoint of the channel. The gate electrode is a thin layer of metal of width $2w$ attached to the floor of the channel, whose center is in general located at x_G (in the figure, $x_G = 0$). The theory is developed with the convention that the powered electrode is on the left, but the section concludes with remarks on the effect of switching the powered and grounded electrodes.

When a voltage is applied across the channel (Fig. 2), the resulting electric field forces electrons to migrate in the gate electrode, which causes

the external field lines to perpendicularly intersect the surface of the gate electrode. While this is the steady state solution in vacuum, in an electrolyte these field lines drive positive and negative ions toward the gate electrode surface, thereby charging the induced double layer. Steady state is reached when enough ions have been driven into the double layer to completely screen the gate electrode from the applied electric field. At this point, only the electric field *along* the channel (parallel to the electrode surface) remains in the bulk solution.

This simplified picture describes the response of the double layer to a dc field. A very important characteristic of ICEO is that it generates a steady flow even in an AC field. Since the electric field *induces* the double layer charge, the sign of the charge varies in phase with the direction of the electric field. There is thus a nonzero net force, (which depends on the product of the two), which drives a steady flow. However, it takes time for the double layer to form. For conducting spheres and cylinders, this charging time τ_c is given exactly by

$$\tau_c = \frac{2\lambda_D w}{D}, \tag{4}$$

where D is the ionic diffusivity, and λ_D is the Debye length of the double layer,

$$\lambda_D = \left(\frac{\epsilon_w k_B T}{2 n_0 e^2}\right)^{1/2}, \tag{5}$$

where ϵ_w is the permittivity of the water, k_B is Boltzmann's constant, T is temperature, n_0 is concentration (of a 1:1 symmetric electrolyte), and e

is the electron charge. For a planar gate electrode, there is a spectrum of charging modes, so that Eq. 4 represents a characteristic charging time of the system. When the frequency of the applied potential is much smaller than the charging frequency $1/\tau_c$, the double-layer evolves quasi-steadily: the bulk electric field and the the double layer depend on the instantaneous value of the applied voltage, and not on its prior evolution.

The voltage applied to the powered electrode is given by

$$\phi_D(t) = V_D \sin(\omega t), \tag{6}$$

so the electric field in the channel is approximately uniform and is given by

$$\vec{E}(t) = \frac{V_D}{2L} \sin(\omega t)\hat{x}. \tag{7}$$

The potential in the bulk of the solution thus drops linearly from the powered electrode to the grounded electrode, and is given explicitly by

$$\phi_B(x,t) = \frac{\phi_D(t)}{2}\left(1 - \frac{x}{L}\right). \tag{8}$$

In the quasi-steady limit,

$$\zeta(x,t) = \phi_G(t) - \phi_B(x,t), \tag{9}$$

where the (spatially constant) potential of the gate electrode $\phi_G(t)$ can vary

in time. To determine $\phi_G(t)$, we use a global charge constraint: the field-induced double layer cannot change the total charge in the double layer, only its distribution. Therefore, if we integrate over the entire gate electrode, we require

$$\frac{1}{2w}\int_{x_G-w}^{x_G+w}\zeta(x,t)\mathrm{d}x = \zeta_{eq}, \tag{10}$$

where ζ_{eq} is the equilibrium zeta potential, which is present even in the absence of an applied electric field. Applying this condition to Eq. 9 and solving for $\phi_G(t)$, we find

$$\phi_G(t) = \zeta_{eq} + \phi_B(x_G,t). \tag{11}$$

The zeta potential over the gate electrode can now be written

$$\zeta(x,t) = \zeta_{eq} + \frac{V_D}{2}\left(\frac{x-x_G}{L}\right)\sin(\omega t). \tag{12}$$

The corresponding time averaged flow, given by the Helmholz-Smoluchowski slip velocity, is

$$\langle u\rangle = -\frac{\epsilon_w}{\eta}\langle\zeta(x,t)\vec{E}(t)\rangle = -\frac{\epsilon_w}{2\eta}\left(\frac{V_D}{2L}\right)^2(x-x_G). \tag{13}$$

Note that ζ_{eq} does not affect the flow, since it does not vary in phase with the field. The slip velocity depends on the difference $x - x_G$: no matter where the gate electrode is located, the ICEO slip velocity will look the same. In

addition, the flow is an odd function of $x - x_G$, which means that there should be a perfectly symmetric flow converging on the middle of the gate electrode. Finally, the flow is independent of the bulk potential directly above the gate electrode – and therefore, one would expect the ICEO flow *not* to depend on which electrode is powered and which is grounded.

The above picture, however, takes into account only the potential gradient *along* the channel. We have neglected a rather large conductor that has close proximity to our system: the metallic microscope stage. When we impose the boundary condition that the potential must vary from $\phi_B(x_G, t)$ in the channel to $\phi_S(t)$, the potential of the stage, we immediately break the symmetry of the system. The stage is typically grounded, and we now have to consider the effects of this vertical (i.e. perpendicular to the surface of the gate electrode) potential gradient (Fig. 3). The gate electrode interacts capacitively with the stage: when the potential in the bulk $\phi_B(x_G, t)$ is positive (Fig. 3(a)), the bottom surface of the gate electrode becomes negatively charged. Because the area of the gate electrode is so small, one would expect the capacitive interaction with the stage to be inconsequential, and not yield observable consequenses. However, the gate electrode often extends past the walls of the channel (Fig. 1(a)), which increases the capacitive coupling to the stage, and thereby causes a significant amount of charge to migrate to the bottom surface of the gate electrode. Because the global charge balance still applies to the gate electrode, this vertical charge migration will cause negative charges to accumulate at the top surface of the gate that is in con-

tact with the electrolyte. In response, a positively charged "stray" double layer forms in the fluid above the gate, which is then driven towards the grounded driving electrode. When the electric field switches direction, the stray double layer becomes negatively charged, so the fluid continues to flow towards the grounded driving electrode (Fig. 3(b)).

To determine the amount of charge in the stray double layer, we model the potential drop from the bulk solution to the stage as taking place over two capacitors in series. The first capacitor is the stray double layer itself, which consists of a layer of ionic charge and the top surface of the gate electrode. The capacitance of the double layer, in the Debye-Huckel ($\zeta \ll 1$) limit, is

$$C_{DL} = \frac{A_G \epsilon_w}{\lambda_D}, \tag{14}$$

where A_G is the area of the gate electrode (in contact with the electrolyte), and ϵ_w is the electric permittivity of the electrolyte. (In the experiments, $\lambda_D \sim 30$ nm and $A_G = 1.5 \times 10^4$ μm^2.) The voltage drop across the stray double layer, from the bulk to the gate electrode, is given by $-\zeta_S$ by definition. The second capacitor is modeled as a parallel plate capacitor between the bottom surface of the gate electrode (including any area that extends beyond the channel walls) and the microscope stage. The glass slide occupies the space between the two plates. Thus, the capacitance of this stray capacitor is

$$C_S = \frac{A_P \epsilon_g}{d}, \tag{15}$$

where A_P is the area of the metal pads (plus the area of the gate, which is a negligible correction), $\epsilon_g = 4.6$ is the electric permittivity of glass (pyrex, Corning), and $d = 1$ mm is the thickness of the glass slide. The potential drop across both capacitors is the difference between the bulk potential directly above the gate electrode $\phi_B(x_G, t)$ and the potential of the stage ϕ_S. Although typically the stage is grounded, in the experiments we allow it to take on any voltage with the same frequency and phase as the driving potential, so

$$\phi_S(t) = V_S \sin(\omega t). \tag{16}$$

Imposing the condition that the total charge on both of the capacitors in series is equal yields

$$\zeta_S(t) = -\frac{\phi_B(x_G, t) - \phi_S(t)}{1 + C_{DL}/C_S}. \tag{17}$$

The electric field drives this double layer just like any other, generating a "stray" fluid slip velocity given by the Helmholz-Smoluchowski relation

$$u_S(t) = -\frac{\epsilon_w \zeta_S(t)}{\eta} E_\parallel(t). \tag{18}$$

Only the time average of the flow is experimentally measurable, and it is given by

$$\langle u_S \rangle = \frac{\epsilon_w V_D \left(\frac{1}{2} V_D (1 - x_G/L) - V_S\right)}{4\eta L (1 + C_{DL}/C_S)}. \tag{19}$$

In what follows, we describe experiments that test Eq. (19) in three ways:

controlling V_S, changing C_S (by varying the area of the metal pads), and moving x_G. Importantly, the standard ICEO characteristics of the system are theoretically unaffected by these parameters.

Finally, we have assumed in the above derivation that the powered electrode was on the left, and the grounded electrode was on the right. Switching the leads to the powered and grounded electrodes reverses the direction of the stray flow, although this is not obvious from Eq. (19). To make this clear, let us choose $x_G = 0$ for simplicity, so that $\phi_B(x_G, t) = \phi_D(t)/2$ remains unchanged by switching the leads. In the experiments, one of the electrodes is powered and the other is grounded, but it is instructive to consider the left electrode at a potential

$$\phi_L(t) = V_L \sin(\omega t) \tag{20}$$

and the right electrode at a potential

$$\phi_R(t) = V_R \sin(\omega t). \tag{21}$$

In this case, the electric field is

$$\vec{E}(t) = \frac{V_L - V_R}{2L} \sin(\omega t)\hat{x}, \tag{22}$$

and the potential above the gate is

$$\phi_B(x_G = 0, t) = \left(\frac{V_L + V_R}{2}\right) \sin(\omega t). \tag{23}$$

The stray slip velocity is then given by

$$\langle u_S \rangle = \frac{\epsilon_w \left(V_L - V_R\right)\left(\frac{V_L+V_R}{2} - V_S\right)}{4\eta L(1 + C_{DL}/C_S)}. \tag{24}$$

Equation (24) shows that switching the powered and grounded electrode will reverse the direction of the asymmetry; if the stage is grounded ($V_S = 0$), then the stray flow will always be directed towards the grounded electrode (see online video 1, where we do this). If $x_G \neq 0$, then the stray flow still switches directions upon flipping the leads, but the magnitude also changes since x_G effectively becomes $-x_G$, so $\phi_B(x_G, t)$ takes on a different value (see online video 2).

3 Experimental Methods

3.1 Device fabrication

The gate electrode is patterned onto the glass slide using standard soft lithography procedures. The glass slide (Corning 2947-75x50) is first cleaned in piranha solution (3:1 H_2SO_4:H_2O_2), followed by a dehydration bake at 200°C for 5 minutes. The slide is then first spin coated with hexamethyldisilazane (HMDS) (Microchem), followed by AZ5214 photoresist (Microchem), both at 4000 rpm for 30 seconds. This is followed by a soft bake at 95° C for 1 minute. The slide is exposed to UV at 7.5mW/cm^2 for 10 seconds, under a high resolution (20000 dpi) transparency mask (CAD/Art Services, Inc.),

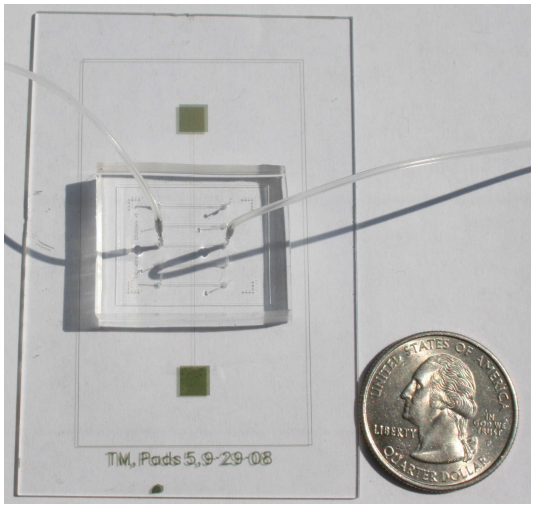

Figure 4: The final device, including gate electrode, channels, access pins, and tubing.

after which it must be reverse baked at 110° C for 1 minute. Finally, the slide is flood exposed for 1 minute, then developed in MF-701 developer for 45 seconds with agitation. A 5 nm layer of titanium was deposited by e-beam assisted Joule evaporation at 0.5 Å/s, followed by a 20 nm layer of gold at 1 Å/s. The resist was removed by lift-off in acetone in an ultrasonic bath. The slide was stored in a container (Fluoroware) for not more than two days before running experiments, in order to prevent significant amounts of contaminant from building up on the gate electrode over time.

The channels are fabricated by casting poly(dimethylsiloxane) (PDMS) against a master mold in a procedure very similar to that described in [27]. The mold starts as a 3" Silicon wafer with a thick oxide ($\sim 80\mu$m) grown on it. The channels are patterned onto the wafer with the same lithography

procedure described above (except only a 7 second exposure is needed), up to and including the develop step. The wafer is then dipped in HF for 3 minutes, followed by an acetone/isopropanol lift-off. This is followed by an 80 minute Bosch etch and another 3 minute HF rinse. The mold is finished after an 8 minute piranha etch.

The PDMS (Motive RTV615) is poured in the ratio 10A:1B, and placed in a planetary mixer (Thinky ARE-250) for 1 minute at 2000 rpm, followed by a 2 minute defoaming at 2200 rpm. The mold is exposed to tridecafluoro-1,1,2,2-tetrahydrooctyltrichlorosilane (Gelest) for 30 minutes under a vacuum desiccator to make the surface hydrophobic (this step is only necessary the first time a mold is used). The mold is placed in a Petri dish covered in alumnium foil. The PDMS is then poured over the mold, placed under vacuum for 1 hour to remove bubbles, then baked at 80°C for 1 hour. The PDMS is then cut to size, and access holes to the channels are punched using gauge 26 luer stub adapters (McMaster-Carr). The surfaces are cleaned with scotch tape.

To bond PDMS to glass, the PDMS is placed in a photo-ozone reactor for 5 minutes in order to oxidize the surface. Also, the glass slide is cleaned with acetone followed by isopropanol in an ultrasonic bath for two minutes each, after which it is placed under oxygen plasma for 30 seconds. The PDMS is aligned over and pressed onto the glass slide, then baked at 120° C for 20 minutes. Hollow stainless steel pins (New England Small Tube) are inserted into the access holes, and 15 cm segments of microline tubing (Silastic) are

connected to the pins. One particular device is shown in Figure 4. All experiments were run immediately following the fabrication of the device.

3.2 Data collection

The device is first taped securely onto the stage of an inverted epifluorescence microscope (Nikon Eclipse TE2000-U). A 100 μM KCl solution is prepared from Milli-Q® water (Millipore), and 0.02% wt. 500 nm diameter fluorescent beads (Bangs Laboratories FS03F) are added for flow visualization. Electrolyte is introduced into the channel by hand using a luer-lock syringe (BD) attached to the microline tubing. Once the electrolyte fills the channel, the two pieces of microtubing attached to each of the pins are submerged in a small beaker filled with the electrolyte. While submerged, the microtubing is carefully removed from the syringe using tweezers, preventing stray pressure gradients and air bubbles from entering the tubing, thereby halting any pressure driven flow. The tracer particles are illuminated with light from a mercury lamp (Nikon C-SHG1) that passes through a B-2E/C dichroic fluorescence filter. A highly sensitive, backlit EMCCD fluorescence video camera (Andor iXon, Model DV885KCS-VP) is used to record the image, and all image capturing was handled with the accompanying Andor Solis software.

To generate the electric field in the channel, a function generator (Agilent 3320A) was run through a 100x voltage amplifier (Trek PZD350 M/S), and the leads were connected to the driving electrodes. To control the stage

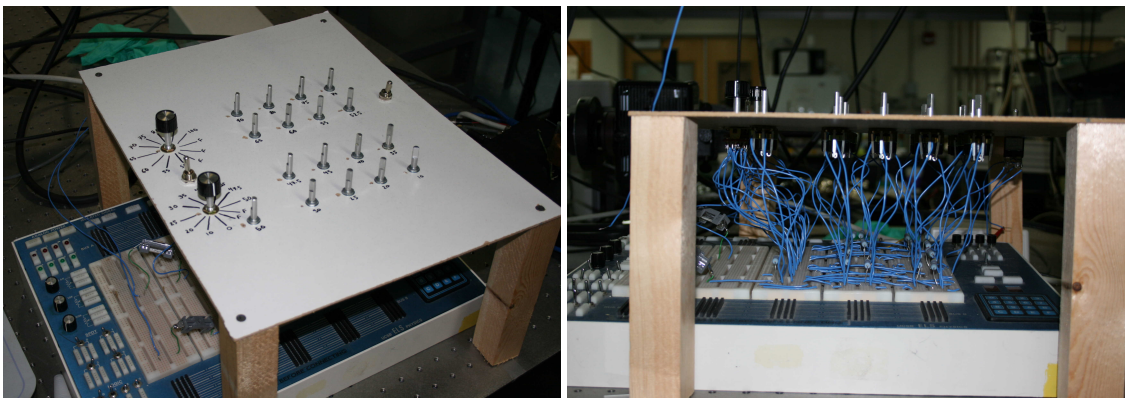

(a) (b)

Figure 5: (a) Isometric and (b) side view of the board of voltage dividers used to drive the stage voltage.

voltage V_S, the driving potential was additionally applied to nineteen resistive voltage dividers (each consisting of a 4.7 kΩ resistor and a 10 kΩ potentiometer), shown in Figure 5. The dividers could be quickly switched between using a manual rotary switch. The stage and objective lens casings were powered from these voltage dividers, but caution is needed to make sure the microscope is not connected to electrical ground. Additionally, the stage was electrically isolated from the objective casing by placing scotch tape over the metal extensions on which the stage rests. In the majority of experiments, when $x_G = 0$, the one half voltage divider was connected to the objective lens in order to isolate the stage as the only contributor to the stray capacitance.

A sequence of simple steps was followed to record a video of the fluid

flow. First, the optical shutter was opened (the shutter was closed between videos to prevent photobleaching of tracer beads). The electric field was then turned on, and a video was immediately recorded. All videos were captured in frame transfer mode for 130 frames, with an exposure time of 0.03441s (26.199 frames per second), the baseline clamp on, and no gain. The electric field was turned off and the shutter was closed immediately following video capture.

3.3 Velocity measurements

The velocity of the fluid flow was determined by micro particle image velocimetry (μPIV), which uses a correlation algorithm to analyze the motion of the fluorescent tracer particles in two successive frames (Fig. 6(a)) of a video, and thereby deduce a 2D velocity field [28, 29]. The algorithm divides the images into "interrogation regions" and determines a velocity vector for each such region (Fig. 6(b)). This is done by shifting the first frame relative to the second in both the x and y directions, and determining a correlation value for each shift. The correlation value is essentially the matrix dot product of the two frames: because beads are white (and therefore are represented by larger values than the black background), the correlation value will only be large when the first frame is shifted a distance such that its beads overlap with the beads of the second frame. A correlation function mesh plot for one interrogation region is shown in Figure 6(c), after averaging over all 129 frame pairs. So far, the resolution of this method is limited to one pixel

(~ 0.358 μm in our case). However, the mesh plot is then fit to a Gaussian, and the displacement of the beads is taken to be the location of the peak of the Gaussian. This allows for sub-pixel accuracy in determining the displacement. The velocity vector is calculated by dividing this displacement by the time between frames. In our case, the frame was 512 x 256 pixels, and the interrogation regions were 128 x 32 with 75% overlap. The μPIV algorithm ensemble averages over the 129 frame pairs of each video to produce the final vector field (Fig. 6(d)).

The slip velocity at a given x-position of the gate electrode is calculated by averaging over the x-components of velocity at each position of y. The error bars in Fig. 7(a) reflect the standard deviation of this data set. The y-component of velocity, in the plane of the gate electrode and perpendicular to the electric field, can be attributed to the Brownian motion of the tracer particles between video frames and is neglected. Because the ICEO flow creates two counter-rotating rolls of fluid above the gate electrode, there is a nontrivial velocity component in the z-direction, out of the plane of the gate electrode. This velocity component is greatest at the location where the ICEO flow converges, which, for a symmetric flow, is near the middle of the gate electrode. The geometry of the optical set-up precluded the measurement of this velocity component. The quantity of interest, however, is the slip velocity of the fluid directly outside the double layer, which is primarily in the x-direction, and which is measured in our experiments.

The error in the x-component of the velocity due to Brownian motion of

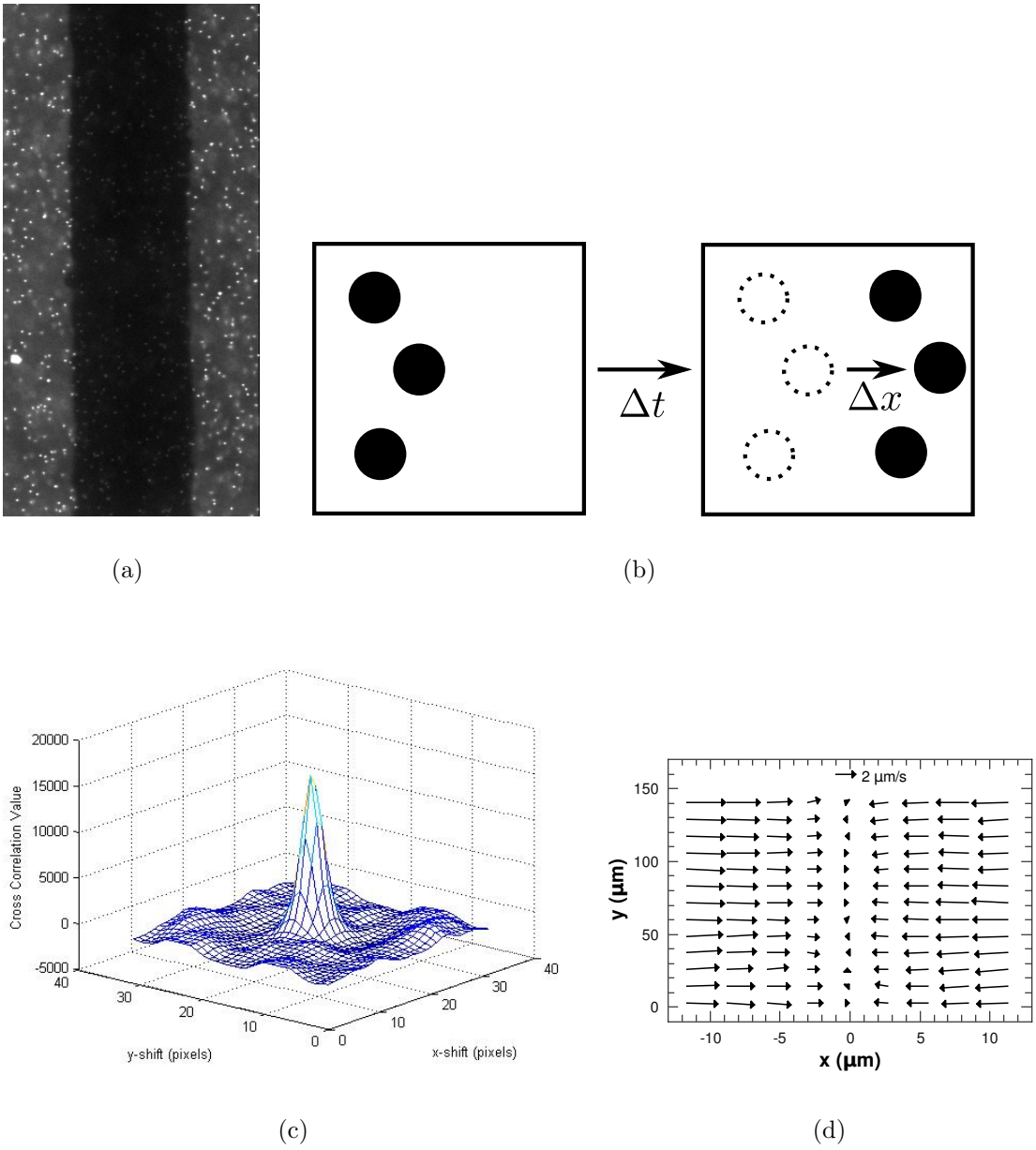

Figure 6: The essentials of PIV. (a) A frame from an ICEO video. (b) Demonstration of the correlation process on one interrogation region in two successive frames. (c) A mesh plot of the correlation values for a 32x32 pixel interrogation region. (d) A vector field produced for one ICEO experiment.

the tracer particles can be estimated by calculating the root mean square displacement of a tracer particle divided by the time between consecutive frames [29]. Thus, the absolute error in velocity associated with Brownian motion of a single tracer particle is estimated by

$$\varepsilon_B = \sqrt{\frac{2k_BT}{3\pi\eta d\Delta t}}, \tag{25}$$

where it is assumed that the diffusion coefficient of the tracer particle is given by the Stokes-Einstein relation, where k_B is the Boltzmann constant, T is the temperature of the electrolyte (assumed 300K), η is the dynamic viscosity of the electrolyte (assumed to be that of pure water, 0.89 cP[30]), d is the diameter of the tracer particles (500 nm), and Δt is the time between successive frames (0.038 s). Since the Brownian displacement is randomly distributed over all directions, it can be reduced by averaging over many tracer particle images. The Brownian error then goes like $\varepsilon_B/\sqrt{N}$, where N is the number of particle images in the average. In the experiments, the velocity data are ensemble averaged over 129 frame pairs, and there are at least 10 tracer particles in each interrogation region, so we take $N = 1290$. The error in the x-component of the velocity due to the Brownian motion of the tracer particles is estimated to be 0.2 μm/s.

Additional sources of uncertainty include the precise location of the focal plane, and the 4.3 μm depth of focus of the optical system (Objective, Nikon Plan Fluor 20x, NA=0.45; CCD, 8 x 8 μm pixel size). Using bright-field il-

lumination, we initially focus on the edge of the electrode, locating the focal plane to within ± 4 μm of the electrode surface. Furthermore, particles that are out of focus contribute to the PIV correlation via a weight $\epsilon(z)$ that is sharply peaked at the focal plane, and falls to 1% over a distance z_{corr}, which for our experiment is approximately 4.5 μm [20, 31]. In order to ensure a sufficient number of tracer particles appear within the focal plane, we use the fine focus to raise the focus 4 μm above the electrode. Captured images thus represent a focal volume approximately 4 μm thick, centered 4 ± 4 μm above the electrode, and velocities measured with μPIV represent *weighted averages* over this volume. A slip velocity $u_s(x)$, over an electrode of half-width L, drives counter-rotating vortices whose vertical scale is (roughly) set by the half-width L. Velocity gradients thus scale like $\partial u_x/\partial z \sim u_s(x)/L$, so that the velocity a distance z above the electrode is approximately given by $u_x(z)/u_s(x) \sim \mathcal{O}(z/L)$. Significantly, because $z \ll L$ (*i.e.* the distance between the focal plane and the electrode is small relative to the gradient length scale L), we argue that these uncertainties affect the *magnitude* of the measured velocity profile via a multiplicative constant, but not the features we report here. (Note variations *across* the correlation depth are approximately linear, and since $z_{\text{corr}} \ll L$, z_{corr} does not appreciably affect the average.) That is, a linear slip velocity profile *at* the electrode will be measured by μPIV as a linear velocity profile *above* the electrode. Furthermore, the location of the stagnation point (where $u_x = 0$) should be correctly recovered with the μPIV algorithm.

The gate electrode on the photolithography mask is 50 μm wide, yet the photomask resolution results in an electrode whose width in practice ranges from 41-46 μm. The velocity data is typically only reliable at least one interrogation region width (32 pixels $\sim$ 11.44 μm) from the edge of the gate electrode; therefore, velocity data is only presented for the central 23 μm of the gate. Given that our focus is $z \sim 4 \pm 4$ μm above the electrode, and $L \approx 20$ μm, measured velocities are $\approx$ 20-40 % lower than the true slip velocity $u_s(x)$. Our goal in this work is not quantitative agreement between theory and experiment. Rather, we seek to measure how the stray velocity due to capacitive coupling with the microscope stage depends upon V_S, C_S and x_G. Our central conclusions rest upon comparisons of measured velocities *relative* to each other, which effectively normalizes away any systematic error that occurs in the *absolute* velocity measurement.

4 Results

4.1 Effect of Stage Potential

The stray flow can be robustly controlled by varying the potential of the microscope stage. Figure 7(a) shows the fluid velocity (due to both ICEO and stray effects) as a function of position along the gate electrode, for various values of V_S. The device used in these experiments had pad area $A_P = 10.0352$ mm^2. It is convenient to quote the pad area in terms of its direct effect on ζ_S, and for that purpose we refer to a scaled pad area $\tilde{A}_P \equiv (1 +$

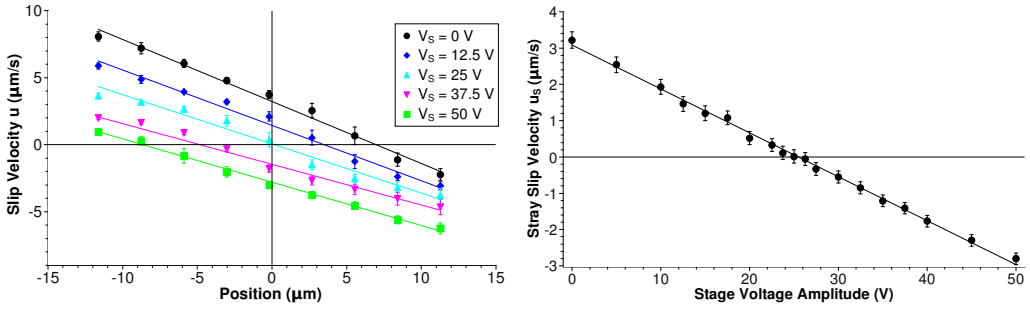

(a) (b)

Figure 7: Effect of stage potential on stray ICEO flow. The scaled pad area is $\tilde{A}_P = 0.00115$, the gate is located at $x_G = 0$, the electric field amplitude is 50 V/cm and the frequency is 100 Hz. (a) The net fluid velocity over the gate electrode is shown for representative stage voltage amplitudes V_S. As stage voltage increases, the velocity over the whole gate decreases by an amount that is independent of position. The slope of the lines, which is due to standard ICEO, is unaffected by stage voltage. (b) The stray flow over the gate electrode is shown as a function of stage voltage. Importantly, the stray flow is essentially 0 um/s when $\phi_B(x_G, t) = \phi_S(t)$ ($V_S = 25$), and the stray flow switches directions once V_S exceeds this voltage.

$C_{DL}/C_S)^{-1}$, here 0.00115. The powered electrode is driven with a signal amplitude of 50 V, resulting in an electric field in the channel of 50 V/cm. The gate electrode is located at $x_G = 0$, and therefore the potential in the bulk directly above the gate has amplitude $V_B = 25$ V. As V_S increases from 0 to 50 V, the velocity of the fluid over the gate decreases uniformly (that is, the decrease in velocity is independent of position). This strongly supports the notion that the stray flow is superposed on the symmetric, standard

ICEO flow. The net fluid velocity over the gate electrode can be written as

$$\langle u(x) \rangle = -\frac{\epsilon_w |\vec{E}|^2}{\eta}(x - x_G) + u_S. \tag{26}$$

The effect of varying V_S is only to alter the stray component u_S. The slope of the curves, given theoretically by $\epsilon_w |\vec{E}|^2/\eta$, is determined only by the standard ICEO characteristics of the system, and the experiments confirm that this slope is unaffected by V_S. This allows us to easily infer the stray flow component by

$$u_S = u(x_G). \tag{27}$$

In other words, the stray flow is equal to the flow at the center of the gate electrode, where the standard ICEO flow vanishes. In this manner, the stray flow was deduced from the linear regressions of plots like those in Fig. 7(a), and the results are shown in Fig. 7(b). The error bars in Fig. 7(b) represent the uncertainty in the flow velocity due only to the uncertainty in the location of the center of the gate electrode ($\sim 1\mu$m). This demonstrates the linear dependence of u_S upon V_S, as predicted by Eq. 19. Notably, the stray flow vanishes when the stage voltage is equal to the bulk voltage above the gate ($V_S = 25$). This demonstrates an effective method of restoring the symmetry. As V_S increases past this value, the stray velocity begins to grow in magnitude, but now it is directed toward the powered electrode. The qualitative features of the observed behavior perfectly match the predicted consequences of the stray capacitance theory.

4.2 Effect of location of gate electrode

The effect of moving x_G is to change the potential drop $\phi_B(x_G, t) - \phi_S(t)$, and it therefore has similar consequences as changing V_S, described above. Figure 8 shows the fluid velocity over the gate electrode for $x_G = 0.33$ cm and

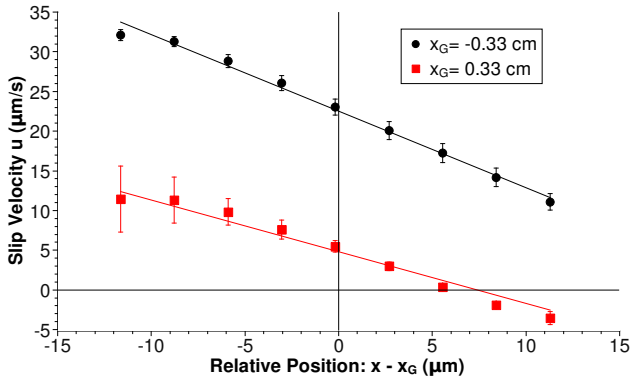

Figure 8: Effect of gate electrode location on stray ICEO flow. The pad area is $\tilde{A}_P = 0.00115$, the stage is grounded ($V_S = 0$), the electric field amplitude is 50 V/cm and the frequency is 100 Hz. The net fluid velocity over the gate electrode is shown for $x_G = 0.33$cm and $x_G = -0.33$cm. The stray flow is deduced from $u_S = u(x = x_G)$. By Eq. 19, the stray flows should be different by a factor of $1.66/0.34 = 4.9$, and experimentally the ratio is $22.5/4.7 = 4.8$. The relative magnitudes of the stray flow are in great agreement with theory.

$x_G = -0.33$ cm. In this experiment, $\tilde{A}_P = 0.00115$, $V_S = 0$ (stage grounded), and $E = 50$ V/cm. Again, the two curves have the same slope (to within experimental error). The stray flow is deduced from the linear regression to be $u_S = 22.5\mu$m/s when $x_G = -0.33$ cm, and $u_S = 4.7\mu$m/s when $x_G = 0.33$ cm. The ratio of the stray flow speeds is then 4.8, in excellent agreement with the predicted value of 4.9, which comes from Eq. 19.

4.3 Effect of pad size

We have shown thus far that some electrical interaction with the microscope stage is certainly responsible for the stray flow, but not that it is necessarily mediated by the pads attached to the gate electrode. In Fig. 9, the stray flow velocity is plotted against the scaled pad area, with $V_S = 0$, $x_G = 0$,

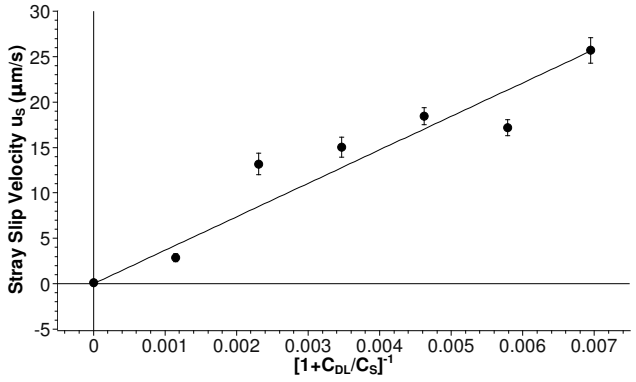

Figure 9: Effect of pad size on stray ICEO flow. The position of the gate is $x_G = 0$, the stage is grounded ($V_S = 0$), the electric field amplitude is 50 V/cm and the frequency is 100 Hz. The error bars denote the combined uncertainty in the location of the center of the gate electrode, together with the standard deviation of the results of 5 identical experiments. The magnitude of the stray flow tends to increase with pad size, as predicted.

and $E = 50$ V/cm. The error bars represent the combined uncertainty in the stray flow due to the uncertainty in the location of the center of the gate electrode (~ 1 μm), and the deviation in the data collected from five identical experiments. Importantly, the stray flow is eliminated when the pads are removed (whereupon $\tilde{A}_P \ll 1$). The stray flow increases approximately linearly with $\tilde{A}_P$, as expected.

5 Discussion

The qualitative results of our experiments strongly support the simple theory we developed. We have demonstrated that the magnitude and direction of the stray flow can be easily manipulated by controlling the potential of the microscope stage. In addition, we have shown that the stray flow increases with increasing pad size, and that removing the pads eliminates the stray flow completely. Furthermore, we have shown that the magnitude of the stray flow depends on the location of the gate electrode in the channel.

The effect of mutual capacitive coupling plays a role analogous to fixed-potential ICEO [9], where the potential of the (metal) inducing surface is forced to vary in phase with the field. Here, however, the gate voltage varies *naturally* due to the capacitive coupling, rather than due to active conrol. The stray capacitance, nonetheless, causes a uniform potential on the gate to vary in phase with the driving field. The flow-FET [22, 25, 26] also involves a ζ-potential that is modulated using an external potential, with an *external* gate electrode playing the role of the stage, and no internal gate electrode. Several differences then arise: modern flow-FETs employ a thin oxide layer upon the electrode, whose acid sites give rise to a high buffer capacitance [32] in parallel with the double-layer capacitance, and thus reduce ζ. Second, the internal gate electrode in our system allows greater geometric variation (*e.g.* connecting to pads outside of electrical contact), giving greater control over C_S and thus flow. A high stray capacitance C_S can be achieved with a

large pad area A_P, whereas the double-layer capacitance exists only over the gate/electrolyte contact area A_G. Because the *total* charge on the gate is constant, ζ_S is geometrically amplified ($C_{DL}/C_S \propto A_G/A_P$).

The absolute magnitudes of both the standard and stray slip velocities are much smaller than their respective theories predict. This is a typical, though poorly understood feature of ICEO flows, and warrants further investigation [20]. In all of the experiments, the applied electric field was 50 V/cm at 100 Hz. At $x = -11.5$ μm (the greatest distance from the center of the gate for which velocities can be reliably calculated), the standard induced zeta potential amplitude is $\zeta_i = 57.5$ mV, and should generate a slip velocity $u = 102$ μm/s. If we extrapolate the standard ICEO flow component from the data (by ignoring u_S), we typically measure slip velocities in the range of 3.7 to 9.2 μm/s. The standard ICEO theory overpredicts the experimental data by a factor between 11 and 28.

For pad size $\tilde{A}_P = 0.00115$, the stray double layer has zeta potential amplitude $\zeta_S = 28.75$ mV, and the expected stray slip velocity is 51 μm/s. The experimentally determined stray flow is $u_S = 3$ μm/s. Similar calculations for the other pad sizes shows that our theory overshoots the experimental data by a factor between 8 and 17.

Of course, approximations are made in the theory that are not necessarily compatible with the conditions of the experiment. For one, the linear Debye-Hückel theory is only valid for $\zeta \ll kT/e \approx 26$ mV, and in our experiments both the standard and stray zeta potentials frequently exceed this value,

although not dramatically. Other assumptions made in our theory are fairly standard (although perhaps incorrect): (i) the gate electrode is clean and smooth, (ii) the double-layer forms fully and quasi-steadily, (iii) Stern layers do not form, (iv) no faradaic reactions occur, (v) ions are point-like and respond to the mean electrostatic field (i.e. Poisson-Boltzmann equation), and (vi) the fluid behaves as a homogeneous continuum.

Because this quantitative discrepancy has been observed frequently in other ICEO experiments [33], we believe that the missing bit of physics responsible for explaining the discrepancy has more to do with general features of electrokinetic and ICEK systems than our specific geometry. To account for this (uniform) quantitative discrepancy between our data and theory, we have normalized our measurements by a common relative velocity. With this normalization, our theory correctly predicts how the stray flow should scale as various parameters – stray capacitance (via pad size), electrode location, stage potential, which electrode is powered – are varied. However, the fact that our theory shares the same margin of error in predicting the results of experiments as a previously existing theory is not a rigorous proof that the same missing bit of physics, once discovered, will correct both of the theories. For example, it has been argued that any contaminant on the gate electrode acts as an additional capacitor C_d in series with the double layer, reducing the induced zeta potential [9] and thus the slip velocity. Such a contaminant reduces the (symmetric) ICEO flow much more strongly than the stray flow discussed here. The induced ζ driving the symmetric component of the ICEO

flow depends exclusively upon $V_B - V_G$; any dielectric capacitor thus reduces the potential drop across the diffuse layer. By contrast, the induced ζ driving the stray flow depends upon $V_B - V_S$, which already includes the (glass slide) as capacitor. Any additional nanometer-scale contaminant has a negligible effect upon the total dielectric capacitance, and thus upon the stray flow. Therefore, the relatively small magnitude of the measured stray slip velocity cannot be ascribed to a contaminant layer on the gate. Other mechanisms – including steric effects within highly-concentrated double-layers – may play a role [34, 35, 36].

The frequency of the electric field was not varied in these experiments, but rather kept low (100 Hz) to allow the double layer time to fully charge. In standard ICEO, theory predicts that the slip velocity falls with increasing frequency once the "RC" charging time for the surface is exceeded [9], and intuition suggests that the stray flow should behave similarly. The charging time for the stray double layer may differ, however, since ions are brought in from the bulk rather than from from one side of the surface to the other. A study into the frequency dependence of standard ICEO and capacitive ICEO could reveal interesting differences. Similarly, the electric field was held at 50 V/cm for all of these experiments. At higher field strengths (*e.g.* 100 V/cm), we observed the slip velocity profile to saturate towards the edges of the gate electrode, where the ζ_i is highest. We believe that this reflects the onset of more significant nonlinearity in the double-layer, where other effects – *e.g.* steric repulsion between ions, non-continuum effects – may

become important [33]. It is interesting to note, however, that even at a field strength of 50 V/cm, the amplitude of the standard ICEO induced zeta potential at $x = -11.5$ μm, neglecting the stray double layer, is $\zeta \approx 50$ mV, or approximately twice the thermal voltage. Nevertheless, the slip velocity was measured to vary linearly with position along the gate electrode. This linearity was also observed for the variation of stray flow with stage voltage (Fig. 7(b)), for which the stray zeta potential, with $\tilde{A}_P = 0.00115$, reaches $\zeta_S = 28.75$ mV (when the stage is grounded). We chose to gather data using the smallest electric field possible for which the slip velocity was still easily observable.

The asymmetric flow that we have described was a surprise when it was first observed in experiments intended to characterize other facets of ICEO. The fact that it results directly from the experimental apparatus used to measure the flow can render it a troublesome experimental quirk. In fact, mutual capacitive coupling may also be responsible for unexpected observations in electrohydrodynamic experiments [21, 37, 38], in which asymmetric behavior was observed to consistently occur around either a grounded or powered electrode. Understanding this mechanism provides a number of routes to restore the (expected) symmetry. The most obvious solution is to remove any unnecessary "external" conductors: we found that replacing the metal stage with a plastic one drastically reduces the asymmetry, but the contribution of the metal objective casing to the asymmetry can not be similarly removed. In our case, stray flows can be most conveniently eliminated by ensuring the

gate electrode remains mostly confined to the electrolyte, and particularly by not attaching the electrode pads (which are the source of the greatest capacitive coupling to the device's surroundings). In other experiments, where the source of the stray capacitance can not be removed as such, any surrounding conductors should be held at the correct voltage to restore the symmetry in the system. Using a transformer as a phase splitter, the potentials of both electrodes can be driven symmetrically about ground, rather than one electrode being powered and the other grounded, to give $\phi_B(x = 0, t) = 0$. We tested this method on our system and showed that it successfully eliminated the stray flow.

Finally, the capacitive coupling mechanism described need not be exclusively an experimental nuisance, but can in fact be exploited to manipulate double layers and electrokinetic flows over polarizable surfaces. These double layers can be controlled in several simple ways, as we demonstrated, and can generate a robust variety of fluid flows.

Acknowledgements

This work was supported by the National Science Foundation, under CBET CAREER grant 0645097, and REU supplements 0741381 and 0836263. Microfabrication was performed in the UCSB nanofabrication facility, part of the NSF-funded NNIN network. We gratefully acknowledge Steve Wereley, for providing his micro-PIV codes.

References

References

[1] T. M. Squires and S. R. Quake. Microfluidics: Fluid physics at the nanoliter scale. *Rev. Mod. Phys.*, 77(3):977–1026, 2005.

[2] H. A. Stone, A. D. Stroock, and A. Ajdari. Engineering flows in small devices: Microfluidics toward a lab-on-a-chip. *Ann. Rev. Fluid Mech.*, 36:381411, 2004.

[3] R. B. Schoch, J. Y. Han, and P. Renaud. Transport phenomena in nanofluidics. *Rev. Mod. Phys.*, 80(3):839–883, 2008.

[4] J. Lyklema. *Fundamentals of Interface and Colloid Science*, volume 2. Academic Press, London, 1995.

[5] W. B. Russel, D. A. Saville, and W. R. Schowalter. *Colloidal Dispersions*. Cambridge University Press, Cambridge, 1989.

[6] A. Ramos, H. Morgan, N. G. Green, and A. Castellanos. AC electric-field-induced fluid flow in microelectrodes. *J. Colloid Interface Sci.*, 217(2):420–422, 1999.

[7] A. Ajdari. Pumping liquids using asymmetric electrode arrays. *Phys. Rev. E*, 61(1):R45–R48, 2000.

[8] M. Z. Bazant and T. M. Squires. Induced-charge electrokinetic phenomena: theory and microfluidic applications. *Phys. Rev. Lett.*, 92:066101, 2004.

[9] T. M. Squires and M. Z. Bazant. Induced-charge electro-osmosis. *J. Fluid Mech.*, 509:217–252, 2004.

[10] H. Lin, B. D. Storey, M. H. Oddy, C.-H. Chen, and J. G. Santiago. Instability of electrokinetic microchannel flows with conductivity gradients. *Phys. Fluids*, 16(6):1922–1935, 2004.

[11] S. M. Rubinstein, G. Manukyan, A. Staicu, I. Rubinstein, B. Zaltzman, R. G. H. Lammertink, F. Mugele, and M. Wessling. Direct observation of a nonequilibrium electro-osmotic instability. *Phys. Rev. Lett.*, 101(23), 2008.

[12] G. Yossifon and H. C. Chang. Selection of nonequilibrium overlimiting currents: Universal depletion layer formation dynamics and vortex instability. *Phys. Rev. Lett.*, 101(25), 2008.

[13] A. B. D. Brown, C. G. Smith, and A. R. Rennie. Pumping of water with AC electric fields applied to asymmetric pairs of microelectrodes. *Phys. Rev. E*, 63(2):art. no. 016305, 2001.

[14] J. P. Urbanski, J. A. Levitan, D. N. Burch, T. Thorsen, and M. Z. Bazant. The effect of step height on the performance of three-

dimensional ac electro-osmotic microfluidic pumps. *J. Colloid Interface Sci.*, 309(2):332–341, 2007.

[15] V. Studer, A. Pepin, Y. Chen, and A. Ajdari. An integrated AC electrokinetic pump in a microfluidic loop for fast and tunable flow control. *Analyst*, 129(10):944–949, 2004.

[16] J. A. Levitan, S. Devasenathipathy, V. Studer, T. Thorsen, T. M. Squires, and M. Z. Bazant. Experimental observation of induced-charge electro-osmosis around a metal wire in a microchannel. *Coll. Surf. A*, 267:122–132, 2005.

[17] H. Zhao and H. H. Bau. Effect of double-layer polarization on the forces that act on a nanosized cylindrical particle in an ac electrical field. *Langmuir*, 24(12):6050–6059, 2008.

[18] V. A. Murtsovkin. Nonlinear flows near polarized disperse particles. *Colloid J.*, 58(3):341–349, 1996.

[19] N. I. Gamayunov, V. A. Murtsovkin, and A. S. Dukhin. Pair interaction of particles in electric-field. 1. features of hydrodynamic interaction of polarized particles. *Colloid J. USSR*, 48(2):197–203, 1986.

[20] G. Soni. Nonlinear phenomena in induced charge electroosmosis. *Ph.D. thesis*, University of California, Santa Barbara, 2008.

[21] D. A. Saville and J. R. Glynn. Electrohydrodynamic flows in nonhomogeneous liquids. *Ind. Eng. Chem. Res.*, 45(21):6981–6984, 2006.

[22] R. B. M. Schasfoort, S. Schlautmann, L. Hendrikse, and A. van den Berg. Field-effect flow control for microfabricated fluidic networks. *Science*, 286(5441):942–945, 1999.

[23] S. A. Gajar and M. W. Geis. An ionic liquid-channel field-effect transistor. *J. Electrochem. Soc.*, 139(10):2833–2840, 1992.

[24] K. Ghowsi and R. J. Gale. Field-effect electroosmosis. *J. Chromatogr.*, 559(1-2):95–101, 1991.

[25] E. J. van der Wouden, T. Heuser, D. C. Hermes, R. E. Oosterbroek, J. G. E. Gardeniers, and A. van den Berg. Field-effect control of electroosmotic flow in microfluidic networks. *Colloid Surf. A-Physicochem. Eng. Asp.*, 267(1-3):110–116, 2005.

[26] E. J. van der Wouden, D. C. Hermes, J. G. E. Gardeniers, and A. van den Berg. Directional flow induced by synchronized longitudinal and zeta-potential controlling ac-electrical fields. *Lab Chip*, 6(10):1300–1305, 2006.

[27] D. C. Duffy, J. C. McDonald, O. J. A. Schueller, and G. M. Whitesides. Rapid prototyping of microfluidic systems in poly(dimethylsiloxane). *Anal. Chem.*, 70(23):4974–4984, 1998.

[28] S. Devasenathipathy, J. G. Santiago, S. T. Wereley, C. D. Meinhart, and K. Takehara. Particle imaging techniques for microfabricated fluidic systems. *Exp. Fluids*, 34(4):504–514, 2003.

[29] J. G. Santiago, S. T. Wereley, C. D. Meinhart, D. J. Beebe, and R. J. Adrian. A particle image velocimetry system for microfluidics. *Exp. Fluids*, 25(4):316–319, 1998.

[30] CRC Handbook of Chemistry and Physics, 89^{th} edition, 6-175, 2008–2009.

[31] M. G. Olsen and R. J. Adrian. Out-of-focus effects on particle image visibility and correlation in microscopic particle image velocimetry. *Exp. Fluids*, 29(7):S166-S174, 2000.

[32] R. E. G. van Hal, J. C. T. Eijkel, and P. Bergveld. A general model to describe the electrostatic potential at electrolyte oxide interfaces. *Adv. Colloid Interface Sci.*, 69:31–62, 1996.

[33] M. Z. Bazant, M. S. Kilic, B. D. Storey, and A. Ajdari. Towards an understanding of nonlinear electrokinetics at large applied voltages in concentrated solutions. *Adv. Colloid Int. Sci.*, in press, 2009.

[34] M. S. Kilic, M. Z. Bazant, and A. Ajdari. Steric effects in the dynamics of electrolytes at large applied voltages. i. double-layer charging. *Phys. Rev. E*, 75(2), 2007.

[35] M. S. Kilic, M. Z. Bazant, and A. Ajdari. Steric effects in the dynamics of electrolytes at large applied voltages. ii. modified poisson-nernst-planck equations. *Phys. Rev. E*, 75(2), 2007.

[36] B. D. Storey, L. R. Edwards, M. S. Kilic, and M. Z. Bazant. Steric effects on ac electro-osmosis in dilute electrolytes. *Phys. Rev. E*, 77(3), 2008.

[37] C. L. Burcham and D. A. Saville. The electrohydrodynamic stability of a liquid bridge: microgravity experiments on a bridge suspended in a dielectric gas. *J. Fluid Mech.*, 405:37–56, 2000.

[38] S. Sankaran and D. A. Saville. Experiments on the stability of a liquid bridge in an axial electric-field. *Phys. Fluids A*, 5(4):1081–1083, 1993.